NANO LETTERS

2007
Vol. 7, No. 8
2446−2451

Optical Detection of Ion-Channel-Induced Proton Transport in Supported Phospholipid Bilayers

Tsung-Han (Calvin) Yang,[†] Chanel K. Yee,[†,⊥] Meri L. Amweg,[†] Seema Singh,[‡] Eric L. Kendall,[†] Andrew M. Dattelbaum,[§] Andrew P. Shreve,*[,§] C. Jeffrey Brinker,*[,‡,||] and Atul N. Parikh*[,†]

Departments of Applied Science, Biomedical Engineering, and Chemical Engineering and Materials Science, University of California, Davis, California 95616, Materials Science, Sandia National Laboratories, Albuquerque, New Mexico 87106, Materials Physics and Applications Division, Los Alamos National Laboratory, Los Alamos, New Mexico 87545, and Department of Chemical Engineering, University of New Mexico, New Mexico 87106

Received May 20, 2007; Revised Manuscript Received June 20, 2007

ABSTRACT

The integration of ion-channel transport functions with responses derived from nanostructured and nanoporous silica mesophase materials is demonstrated. Patterned thin-film mesophases consisting of alternating hydrophilic nanoporous regions and hydrophobic nanostructured regions allow for spatially localized proton transport via selective dimerization of gramicidin in lipid bilayers formed on the hydrophilic regions. The adjoining hydrophobic mesostructure doped with a pH sensitive dye reports the transport. The ease of integrating functional membranes and reporters through the use of patterned mesophases should enable high throughput studies of membrane transport.

The development of new responsive materials increasingly relies upon the integration of diverse functions into multicomponent architectures that can be produced using self-assembly or other simple processing methods.[1] Along these lines, the coupling of functions derived from biological membranes[2,3] to functions arising from nanostructured and nanocomposite materials[4,5] is of importance. For example, significant recent advances in engineering ion-channels now enable modulation of ionic and molecular transport.[6,7] However, the integration of methods to maintain functional ion channels on solid supports with methods to transduce channel-mediated transport into a detectable signal is required to enable on-chip and high-throughput studies of membrane transport phenomena.[8] Previous efforts have primarily focused on integrating channel transport with electrical transduction.[9,10] Here, we present a design based on thin-film silica mesophase materials that is amenable to high-density arraying and that combines a region facilitating transmembrane proton transport with a surrounding reporter region containing a fast-response pH sensitive optical probe. This design, integrating optical transduction with ion-channel transport, complements more commonly used electrical transduction, allows for future parallel and stochastic studies of membrane transport, and should prove applicable in functional studies of broad classes of ion-channels using supported membrane configuration.

Our design, illustrated in Figure 1, incorporates several properties that enable proton transport and its optical transduction. The area in which transmembrane transport occurs consists of a supported lipid bilayer[11] formed on a mesoporous silica region of a patterned thin film. Gramicidin, a short helical polypeptide, is present in both leaflets of the fluid bilayer, permitting active ion-channel formation via lateral diffusion and interleaflet dimerization for subsequent proton transport.[12] Each such functional or transporter area is closely surrounded by regions that report on pH changes. These reporter, or transduction, areas consist of the fast-response, pH-sensitive dye fluorescein isothiocyanate (FITC) embedded in a mesostructured, surfactant-containing, silica film.[13] In these regions, membrane transport functions are blocked by the presence of a stable, hydrophobic, self-assembled monolayer on the surface of the silica mesophase. The use of photochemically patterned thin films[14] to provide spatial separation of the reporter region and the transporter region yields the important advantage of allowing the use

* Corresponding author. E-mail: anparikh@ucdavis.edu. Phone: 1 (530) 754-7055. Fax: 1 (530) 752-2444.
[†] University of California, Davis.
[‡] Sandia National Laboratories.
[§] Los Alamos National Laboratory.
[||] University of New Mexico.
[⊥] Present addresss: Amgen Corporation, Thousand Oaks, CA.

10.1021/nl071184j CCC: $37.00
Published on Web 07/13/2007

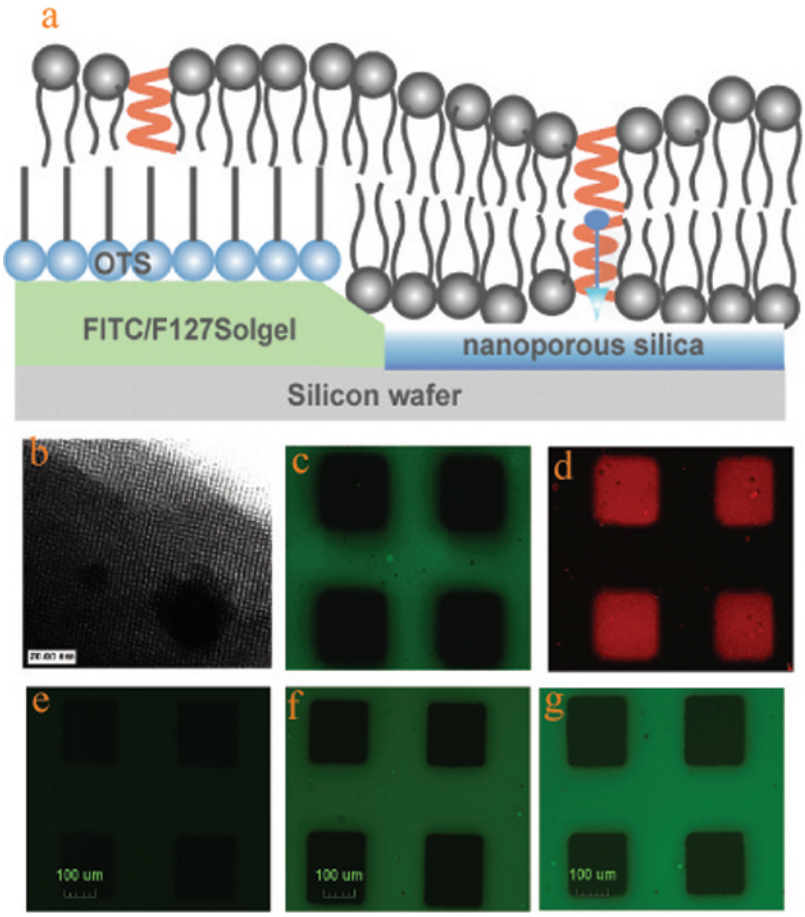

Figure 1. A materials construct for optical transduction of ion-channel-induced proton transport. (a) A schematic depiction of an ion-channel (gramicidin A) containing fluid phospholipid membrane on a FITC-derivatized patterned mesostructure/mesoporous silica thin film. The optical reporter region consists of a FITC-containing mesostructure coated with an *n*-octadecyltrichlorosilane monolayer, and the transporter region is a mesoporous silica substrate. A lipid bilayer in the transporter region enables gramicidin dimerization and subsequent proton transport. A hybrid bilayer in the reporter region effectively blocks the proton transport to the substrate. (b) A cross-sectional TEM image reveals the presence of nanoscale pores in a square-lattice in the transporter regions for photocalcined F127-templated nanoporous mesophase. (c−d) Typical epifluorescence images show the uniform emission from the reporter (green) and transporter (red) regions respectively. (e−g) FITC-derivatized and F127-doped mesophases exhibit solution pH dependent FITC emission (approximately at 1:4:7 for pH 4, 7, and 10), which is in general qualitative agreement with the expected pH dependence of fluorescein.

of mesoporous silica in the transporter region. In contrast to mesostructured regions, which are slightly hydrophobic (water contact angle ~40°) even prior to the addition of the blocking self-assembled monolayer, mesoporous silica provides a fully hydrated and hydrophilic surface (contact angle with water ~0°) for the formation of a stable, uniform and laterally fluid-supported bilayer membrane.[15] Our patterning methods also allow for arraying the entire multifunctional unit in a high-density format, thus facilitating parallel, on-chip, and high-throughput studies of membrane transport phenomena.[8]

We prepare a continuous FITC-derivatized thin-film silica mesophase on a freshly oxidized silicon substrate by adopting a previously reported technique.[13,16] Briefly, 10 mg of FITC in 26 mL of ethanol is mixed with 11 μL of 3-aminopropyltriethoxysilane (APTES) and stirred for ~3 h in the dark. The resulting solution is then added to an acidic aqueous solution of surfactant-doped tetraethylorthosilicate (TEOS). We used a common poly(ethyelene) oxide-poly (propylene) oxide triblock copolymer (pluronic F127) as the organic structure-directing agent. The final composition of the mixture was 1 TEOS:6.3 $\times$ 10^{-4} FITC:1.2 $\times$ 10^{-3} APTES: 10.9 EtOH:2.5 H2O:0.012 HCl:3.9 $\times$ 10^{-3} Pluronics F127 (a tri-block copolymer composed of ethylene-oxide and propylene-oxide blocks, $EO_{100}PO_{65}EO_{100}$). Thin films of FITC-derivatized silica mesophases are then prepared by dip-coating a clean silicon wafer under ambient conditions at a pulling rate of 50 mm/min. After dip-coating, the samples are aged at room temperature in a desiccator for ~4−6 h, followed by a slow-curing at 70 °C for ~2 days. The films are then coated with a monolayer of *n*-octadecyltrichlorosilane (OTS) following a classical solution self-assembly technique.[17] This treatment renders the FITC-derivatized mesophase surface uniformly hydrophobic (water contact angle >100°). Following the OTS assembly, we produce spatial patterns of square-shaped, hydrophilic mesoporous elements by using a previously demonstrated photocalcination procedure in which the sample is illuminated through a photomask using short-wavelength (184−257 nm) UV light.[14] This process removes OTS, the F127 template, aminopropyl groups, and FITC from the exposed areas and promotes further siloxane condensation in the exposed

regions. As suggested in Figure 1, this treatment results in a thinner (determined by aqueous-phase imaging ellipsometry and step-profilometry to be about 35% thinner for typical 400 nm thick films used in our study) nanoporous film bounded by a thicker, F127- and FITC-containing, nanostructured film corresponding to the unexposed regions. The UV-exposed control samples reveal 3.9 nm pore sizes at ~49% porosity in a distorted rectangular arrangement consistent with previous studies, and the FITC-loaded mesostructure is two-dimensional (2D) hexagonal.[18] We confirm that the FITC-containing areas of the patterned film retain their pH-reporting activity[19] by immersing the patterned substrates into aqueous solutions with pH values of 4, 7, and 10 and noting resulting substantial changes in FITC emission intensities (Figure 1e−g). The pH dependent FITC emission intensity within the mesostructured environment demonstrates a fast-response (several seconds) and a sigmoidal-like shape characterized by a rapid intensity rise between pH values of 6.0 and 8. A systematic variation of pH between 2 and 10 produced a complete pH-dependent FITC intensity-based titration curve (Supporting Information). Our titration curve is in a good adgreement with a previous study[13] but shows the inflection point of the sigmoidal at ~7, about 1 pH unit lower probably reflecting small differences in the film structure and preparation conditions. Compared to the solution phase, these reponse curves are broader and probably because of environmental effects[13,20]

The patterned films are subsequently incubated with small unilamellar vesicles (SUVs) consisting of 1-palmitoyl-2-oleoyl-phosphatidylcholine (POPC) lipid, 0.1−0.2 mol % gramicidin, and 1 mol % fluorescent lipid, Texas-red 1,2-dihexadecanoyl-sn-glycero-3- phosphoethanolamine, triethylammonium salt (Texas-red DHPE) to allow visualization of the membranes. Control experiments were performed using identical procedures but with POPC vesicles devoid of gramicidin.

As expected, the surface energy-dependent fusion of SUVs onto these patterned hydrophilic/hydrophobic films results in single lipid monolayers on the reporter (FITC- and F127-derivatized) hydrophobic regions, whereas full bilayers form on the tranporter hydrophilic nanoporous islands of the patterned silica mesophase[21] (Figure 1). Further characterization of these coexisting lipid morphologies is provided below. Assuming all gramicidin is incorporated in the supported membranes (0.1−0.2 mol % or 1.67×10^5 molecules per leaflet within each 100 μm^2 bilayer region) and assuming 0.6 nm^2 area per lipid molecule, the total surface density of gramicidin is estimated as 5.6×10^{-13} mol/cm^2 for both leaflets. Further, the equilibrium association constant of 6.86×10^{14} in mol/cm^2 units[22] indicates that nearly all (~97%) gramicidin molecules within the bilayer regions are dimerized forming functional ion-channels.

Key results obtained are summarized in Figure 2. Fluorescence images obtained using a red emission filter, appropriate for Texas-red DHPE, establish the stability, integrity, and structural consistency of the bilayer in aqueous media at the three pH values examined. The adjustment of aqueous phase pH values was achieved simply by adding controlled amounts of HCl or NaOH to the aqueous phase. Images obtained using a green emission filter appropriate for FITC reveal substantial changes in emission intensity from the reporter region in the presence of gramicidin with an increase of more than a factor of 7 observed between pH values of 4 and 10. In contrast, control experiments confirm that only small changes in FITC emission occur for POPC samples devoid of gramicidin (Supporting Information).

Additional experiments have been performed to validate the primary elements of the structure represented in Figure 1. These are discussed in turn below. First, spatially resolved imaging ellipsometry and step profilometry data confirm that the photopatterned mesophase thin-films display a topographic corrugation: the FITC-doped silanized mesostructure in a representative sample measures at 408 (±4) nm thick film whereas the UV-exposed nanoporous region is 260 (±3) nm thick. These values agree well with 30−35% reduction in mesophase thicknesses upon (photo) calcination reported earlier.[15,23] The transition region between the mesostructure and the mesoporous region yield intermediate values probably because of the thickness gradient within that region. Step-profilometric measurements lend additional support by showing that the transition region represents a continuous variation in film heights between those of mesostructure and the mesoporous regions (Supporting Information). Second, contact angle measurements confirm that photopatterned mesophases are amphiphilic. FITC-doped and OTS-derivatized mesostructure retains high contact angles by water (~104°) whereas the UV-exposed nanoporous region is fully wettable by water (contact angle <10°). Third, the fusion of SUVs on these amphiphilic surfaces (consisting of hydrophobic, FITC-coated reporter mesostructures and hydrophilic nanoporous transporter regions) results in the formation of a complient coexisting monolayer and bilayer morphologies, respectively, consistent with previous reports.[21] This is confirmed using a combination of imaging ellipsometry[24] and fluorescence microscopy[21] methods. An analysis of ellipsometry images reveal 3.7 (±0.3) nm film in the nanoporous region and 1.9 (±0.4) nm in the hydrophobic FITC region in good correspondence with thicknesses of homogeneous lipid monolayers (reporter region) and bilayers (transporter region).[21] The fluorescence images of our samples reveal a bright and homogeneous fluorescence in the mesoporous, transporter regions of the sample, which is consistent with a uniform bilayer formation.[25] The lateral fluidity in this region is verified using fluorescence recovery after photobleaching (FRAP) (Supporting Information). The significantly lower intensity in the reporter mesostructure surroundings (FITC- and F127-doped regions) appears counterintuitive. This apparent discrepancy results from a well-known fluorescence interference effect that arises near a reflective surface.[26] In particular, reflection at the silicon surface produces a standing-wave modulation of the fluorescence intensity as distance perpendicular to the substrate surface is varied.[27] In our case, the topographic corrugation between the transporter and reporter regions places the Texas-red dye in these respective regions at about

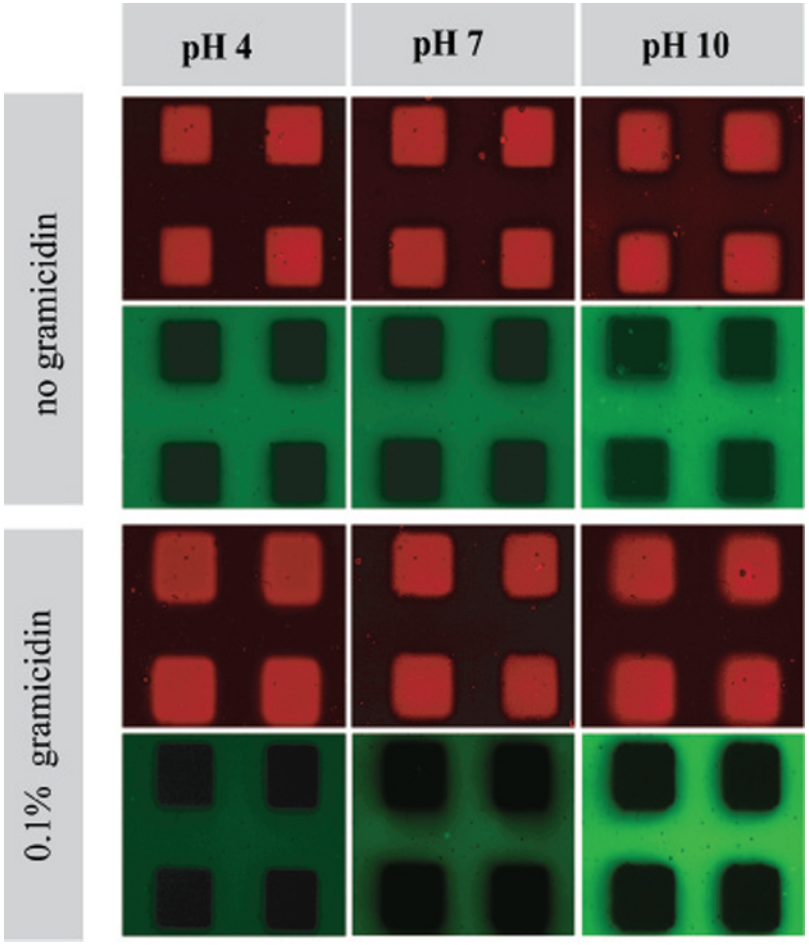

Figure 2. Optical transduction of ion-channel induced proton transport. Red- and green-channel epifluorescence images for a Texas-red DHPE-doped POPC bilayer (top panels) and the same bilayer containing 0.1 mol % Gramicidin A (bottom panels) as a function of solution pH. FITC-containing mesostructure reporter regions appear green and Texas-red DHPE-containing mesoporous transporter regions appear red. The dramatic changes in the FITC emission for the gramicidin containing bilayer reveal an optical response in the mesostructure reporter region induced by the proton transport in the transporter region.

148 nm apart in the *z*-direction, which in turn produces a very low intensity for the monolayer in the reporter region.[26] Circumventing this issue using much lower reflectivity glass as a substrate for the mesophase patterns produces the familiar fluorescence intensity contrast: the bilayer in the transporter region is about 1.7 times more intense than the monolayer.[21] Fourth, because gramicidin dimerization and its transport function depend upon lateral diffusion within the supported bilayer membrane,[9,28] the presence of long-range fluidity in the membrane has been assessed using FRAP measurements. These results confirm $1-2 \times 10^{-8}$ cm^2/s diffusion constants for the Texas-red probe within both the monolayer and bilayer regions consistent with values reported previously.[29]

To establish that the lipid monolayer formed over the OTS-covered reporter regions is laterally connected to the bilayer over the nanoporous transporter regions, we performed a modified FRAP experiment. Here, when all fluorescence emission from a bilayer region in the patterned architectures is photobleached by repeated exposure to an intense excitation beam, subsequent recovery of the fluorescence is observed (Figure 3). Such a recovery necessarily requires the lateral diffusion of unbleached fluorophores from the surrounding monolayer region, indicating a substantial lateral connectivity between the lipid monolayer and the bilayer phases. Previously, by directly patterning OTS monolayers supported on planar glass, we have shown that the lipid monolayers formed on OTS regions are separated from bilayers formed in adjacent glass regions via a $1-2$ μm wide and about 2.4 nm deep moat region that resists vesicle fusion.[21] The absence of such a moat at the monolayer and bilayer transition region corresponding to the deep and broad boundary between OTS-derivatized mesostructure and mesoporous regions can be understood in terms of larger continuous thickness gradient ($\sim 1-10$ um) and possibly a silica-like hydrophilic character of this region thus allowing a smooth morphological transition from lipid monolayer to bilayer (Figure 1).

Further verification of the function of gramicidin and of the means to block transmembrane proton transport in the reporting regions is provided by a series of experiments on uniform (i.e., nonpatterned) mesostructured thin films (Supporting Information). As described above, we prepared a uniform (unpatterned) film in which the silica mesophase

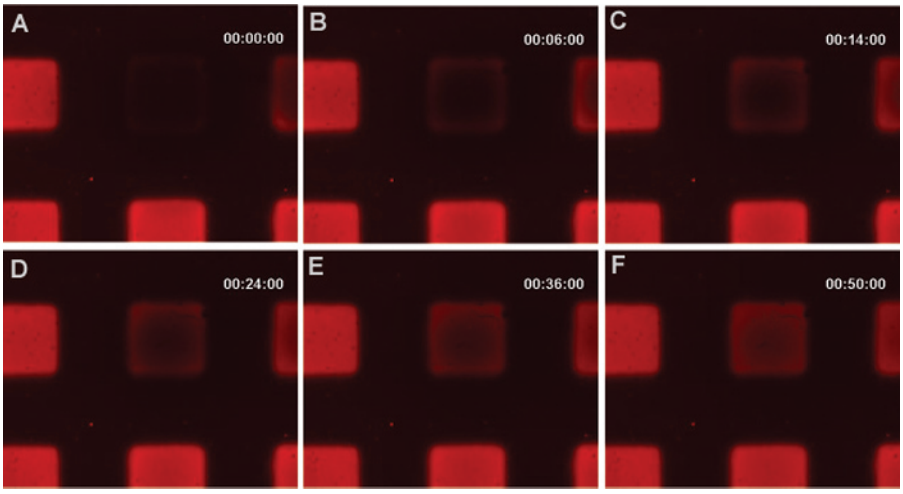

Figure 3. Fluidity, uniformity, and lateral contiguity of the lipid membrane on patterned silica mesophases. Time-lapse fluoresence micrographs from a red-channel movie recorded after photobleaching a gramicidin containing POPC bilayer (doped with 1 mol % Texas-red DHPE) on the mesoporous region of the patterned mesostructure/mesoporous silica film. The square indicated as 1 was fully photobleached by exposures to an intense excitation beam in rapid succession. The recovery of the fluorescence in the bleached area confirms the lateral contiguity and fluidity of the lipid phases. Note also that full recovery of the initial fluorescence is not expected due to the confinement of some permanently bleached Texas-red DHPE molecules in the lower leaflet of the bilayer. The homogeneity of the fluorescence emission from the bilayer and the monolayer areas further confirm their lateral structural uniformities.

material is rendered hydrophobic by self-assembling OTS onto the surface. Spreading of gramicidin-containing POPC vesicles on such a surface leads to a hybrid-bilayer membrane consisting of an OTS monolayer inner leaflet and a POPC monolayer outer leaflet. The gramicidin monomer is confined to the outer leaflet. Varying the solution pH values results in minimal change in the intensity of the FITC fluorescence intensity, indicating that pH equilibration of the mesophase film and the solution does not occur (Supporting Information). Thus, OTS is shown to be effective in blocking transmembrane proton transport.

Taken together, the results reported here confirm the essential features illustrated in the schematic structure in Figure 1. The formation of fluid lipid bilayers in the mesoporous regions of our samples allows trans-leaflet dimerization of gramicidin. These ion-channels then facilitate proton transport across the lipid bilayer. The transported protons are subsequently released in the confined aqueous phase at the interface between the membrane and the mesoporous thin film from where they are able to diffuse into the FITC-doped, surfactant-loaded nanopores of the transducing regions. In contrast, the gramicidin contained in the outer lipid monolayers supported on OTS cannot facilitate proton transport across the entire phospholipid plus OTS hybrid bilayer. It is interesting to note that time-resolved applications of fluorescence measurements reported here may further allow measurements of proton conduction within the mesostructure channels as well as provide a useful means to quantitatively compare the diffusive proton (and ionic) transport through water-filled nanoporous silica compared to that in bulk water ($\sim 9.3 \times 10^{-5}$ cm^2/s).[30] This platform should also allow experiments to test if proton transport is first favored along the lipid headgroup regions before its solvation in the water layer at the membrane−substrate interface.[31]

In summary, we have demonstrated a multifunctional, patterned, thin-film that enables the integration of transmembrane ion transport functions with optical transduction of transport processes. The ease of incorporating various optical (and other) reporters in sol−gel films should allow for detectability of a broad range of ions and molecules. Finally the simplicity of UV photolithography and other patterning methods afford the isolation of single functional units (such as shown in Figure 1) from adjacent ones in a dense pattern. Such simple engineering could enable parallel, stochastic, and high-throughput assays of membrane transport. Future studies in our laboratories are aimed toward these ends.

Acknowledgment. We thank Adrian Brozell for help with fluorescence titration curves. Support for this work was provided by The Office of Science, U.S. Department of Energy and by National Institutes of Health through the NIH Roadmap for Medical Research.

Supporting Information Available: Figures include the design of the membrane platform, frames of gramicidin containing POPC bilayer, epifluorescence images, FTIR microspectroscopy, pH dependent FITC emission intensity response, and results of a preliminary step-profilometry experiment. This material is available free of charge via the Internet at http://pubs.acs.org.

References

(1) Boncheva, M.; Gracias, D. H.; Jacobs, H. O.; Whitesides, G. M. *Proc. Natl. Acad. Sci. U.S.A.* **2002**, *99* (8), 4937−4940.
(2) Edidin, M. *Nat. Rev. Mol. Cell Biol.* **2003**, *4* (5), 414−418.
(3) Vereb, G.; Szollosi, J.; Matko, J.; Nagy, P.; Farkas, T.; Vigh, L.; Matyus, L.; Waldmann, T. A.; Damjanovich, S. *Proc. Natl. Acad. Sci. U.S.A.* **2003**, *100* (14), 8053−8058.
(4) Brinker, C. J.; Lu, Y. F.; Sellinger, A.; Fan, H. Y. *Adv. Mater.* **1999**, *11* (7), 579.

(5) Soten, I.; Ozin, G. A. *Curr. Opin. Colloid Interface Sci.* **1999**, *4* (5), 325−337.
(6) Bayley, H. *Curr. Opin. Biotechnol.* **1999**, *10* (1), 94−103.
(7) Bayley, H.; Jayasinghe, L. *Mol. Membr. Biol.* **2004**, *21* (4), 209−220.
(8) Bayley, H.; Cremer, P. S. *Nature* **2001**, *413* (6852), 226−230.
(9) Cornell, B. A.; BraachMaksvytis, V. L. B.; King, L. G.; Osman, P. D. J.; Raguse, B.; Wieczorek, L.; Pace, R. J. *Nature* **1997**, *387* (6633), 580−583.
(10) Tien, H. T.; Salamon, Z.; Ottova, A. *Crit. Rev. Biomed. Eng.* **1991**, *18* (5), 323−340.
(11) Sackmann, E. *Science* **1996**, *271* (5245), 43−48.
(12) Woolley, G. A.; Wallace, B. A. *J. Membr. Biol.* **1992**, *129* (2), 109−136.
(13) Wirnsberger, G.; Scott, B. J.; Stucky, G. D. *Chem. Commun.* **2001** (01), 119−120.
(14) Dattelbaum, A. M.; Amweg, M. L.; Ecke, L. E.; Yee, C. K.; Shreve, A. P.; Parikh, A. N. *Nano Lett.* **2003**, *3* (6), 719−722.
(15) Clark, T.; Ruiz, J. D.; Fan, H. Y.; Brinker, C. J.; Swanson, B. I.; Parikh, A. N. *Chem. Mater.* **2000**, *12* (12), 3879−3884.
(16) Fan, H. Y.; Lu, Y. F.; Stump, A.; Reed, S. T.; Baer, T.; Schunk, R.; Perez-Luna, V.; Lopez, G. P.; Brinker, C. J. *Nature* **2000**, *405* (6782), 56−60.
(17) Sagiv, J. *J. Am. Chem. Soc.* **1980**, *102* (1), 92−98.
(18) Grosso, D.; Balkenende, A. R.; Albouy, P. A.; Ayral, A.; Amenitsch, H.; Babonneau, F. *Chem. Mater.* **2001**, *13* (5), 1848−1856.
(19) Yguerabide, J.; Talavera, E.; Alvarez, J. M.; Quintero, B. *Photochem. Photobiol.* **1994**, *60* (5), 435−441.
(20) Yang, L.; Saavedra, S. S. *Anal. Chem.* **1995**, *67* (8), 1307−1314.
(21) Howland, M. C.; Sapuri-Butti, A. R.; Dixit, S. S.; Dattelbaum, A. M.; Shreve, A. P.; Parikh, A. N. *J. Am. Chem. Soc.* **2005**, *127* (18), 6752−6765.
(22) Davis, R. W.; Patrick, E. L.; Meyer, L. A.; Ortiz, T. P.; Marshall, J. A.; Keller, D. J.; Brozik, S. M.; Brozik, J. A. *J. Phys. Chem. B* **2004**, *108* (39), 15364−15369.
(23) Lu, Y. F.; Ganguli, R.; Drewien, C. A.; Anderson, M. T.; Brinker, C. J.; Gong, W. L.; Guo, Y. X.; Soyez, H.; Dunn, B.; Huang, M. H.; Zink, J. I. *Nature* **1997**, *389* (6649), 364−368.
(24) Howland, M. C.; Szmodis, A. W.; Sanii, B.; Parikh, A. N. *Biophys. J.* **2007**, *92* (4), 1306−1317.
(25) Doshi, D. A.; Dattelbaum, A. M.; Watkins, E. B.; Brinker, C. J.; Swanson, B. I.; Shreve, A. P.; Parikh, A. N.; Majewski, J. *Langmuir* **2005**, *21* (7), 2865−2870.
(26) Lambacher, A.; Fromherz, P. *J. Opt. Soc. Am. B* **2002**, *19* (6), 1435−1453.
(27) Wong, A. P.; Groves, J. T. *Proc. Natl. Acad. Sci. U.S.A.* **2002**, *99* (22), 14147−14152.
(28) Hwang, T. C.; Koeppe, R. E.; Andersen, O. S. *Biochemistry* **2003**, *42* (46), 13646−13658.
(29) Cremer, P. S.; Boxer, S. G. *J. Phys. Chem. B* **1999**, *103* (13), 2554−2559.
(30) Leung, K.; Rempe, S. B.; Lorenz, C. D. *Phys. Rev. Lett.* **2006**, *96*, 9.
(31) Heberle, J.; Riesle, J.; Thiedemann, G.; Oesterhelt, D.; Dencher, N. A. *Nature* **1994**, *370* (6488), 379−382.

NL071184J